International Journal of GEOMATE, May, 2018 Vol.14, Issue 45, pp.58-65
Geotec., Const. Mat. & Env., DOI: https://doi.org/10.21660/2018.45.7264
ISSN: 2186-2982 (Print), 2186-2990 (Online), Japan

NUMERICAL ANALYSIS ON MECHANISM OF LIQUEFACTION NOT ONLY IN MAIN EARTHQUAKE BUT ALSO IN AFTER SHOCK

*Yukihiro Morikawa[1], Hide Sakaguchi[2], Akihiko Taira[3] and Ho Cho[4]

[1,4] Department of Civil Engineering, Nagoya Institute of Technology, Japan; [2,3] Japan Agency for Marine-Earth Science and Technology, Japan

*Corresponding Author, Received: 9 June 2017, Revised: 27 July. 2017, Accepted: 22 Nov. 2017

ABSTRACT: During the 2011 Great East Japan Earthquake, liquefaction occurred in the reclaimed ground in the wide area of east Japan. In some areas, liquefaction happened in the aftershock was even more serious than what happened in the main shock. For this reason, the liquefaction that happened a long time after the earthquake caused not only by the main shock but also the multiple aftershocks within a short period of time, is intensively investigated in recent years. In this paper, particular attention is paid to the characteristic features of the liquefaction and its consequent consolidation-induced settlement. Based on the observed data, a series of dynamic-static analyses, considering not only the earthquake loading but also static loading during the consolidation after the earthquake shocks, are conducted in a sequential way just the same as the scenario of the earthquake. The calculation is conducted with 3D soil-water coupling finite element-finite difference (FE-FD) analyses based on a rotating-hardening elastoplastic constitutive model. From the analyses, it is recognized that small sequential earthquakes, which cannot cause liquefaction of a ground in an independent earthquake vibration, cannot be neglected when the ground has already experienced the liquefaction after a major shock. In addition, the aftershocks have great influence on the long-term settlement of the soil layers with low permeability. It is confirmed that the numerical method used in this study can describe the ground behavior correctly under repeated earthquake shocks.

Keywords: Repeated earthquake, Liquefaction, FEM, Settlement

1. INTRODUCTION

On March 11, 2011, 14:46:18, 2011 off the Pacific coast of Tohoku Earthquake (The Great East Japan Earthquake) happened with a magnitude of 9.0 in Richter, the greatest earthquake ever recorded in Japan history. Some typical characteristics of the Great East Japan Earthquake can be given, e.g., the duration time of the seismic motion was very long, multiple big aftershocks happened in a relatively short period of time and so on. According to an investigation after the earthquake [1]-[2], the damages due to tsunami and liquefaction were most serious recorded in Japan. Especially multiple aftershocks in a relatively short period of time made damages spread, many existing structures in a wide area along coastal area suffered serious damages. The increase of excess pore water pressure (EPWP) and the development of anisotropy in the ground experienced liquefaction due to the main shock may cause instability of the ground and might cause re-liquefaction in the consequential aftershocks even if the aftershocks are not large. One of the interesting phenomena is that liquefaction not only happened in the main shock of earthquake vibrations but also happened in the first aftershock whose acceleration was much less than that of the main shock. However, it was thought that such a low level of shock was not strong enough to cause liquefaction.

Re-liquefaction happened in a first aftershock was even more serious than what happened in the main shock. This phenomenon indicates a very important fact that the sand boiling was accelerated by the aftershocks and more severe liquefaction occurred during the aftershocks at some sites.

In order to describe and predict correctly the ground behavior in such kind of repeated earthquake vibrations that may occur in future, it is necessary to clarify the mechanism of this geotechnical engineering problem. In this paper, a typical local site of reclaimed ground in Chiba Prefecture Japan is selected for the numerical analyses. Based on the observed data, a series of repeated dynamic-static analyses, considering not only the earthquake loading but also the static loading during the consolidation after each earthquake shock, are conducted in a sequential way just the same as the scenario happened in the Great East Japan Earthquake.

2. CONSTITUTIVE MODEL FOR SOILS AND FINITE ELEMENT METHOD

The numerical analyses and prediction are conducted with 3D soil-water coupling finite element-finite difference (FE-FD) analysis based on the Cyclic Mobility model (CM model) proposed by Zhang et al. [3].

CM model is a kind of rotating -hardening elastoplastic model. It can properly describe the nonlinear behavior of non-cohesive soils under both dynamic and static loadings, especially the cyclic mobility of sand during liquefaction. With CM model and effective stress based FEM code, the mechanical behavior of the ground, such as the change of EPWP, the development of stress-induced anisotropy and the post-liquefaction consolidation, can be properly described not only in the liquefaction stage during the earthquake but also in the post-liquefaction consolidation stage.

Numerical simulation has widely used the analyses of earthquake-induced liquefaction. The object of the numerical simulation or prediction conducted in this paper is to reproduce or predict the overall mechanical behavior during and after the earthquakes, including the liquefaction and consolidation of repeated earthquake vibrations. The simulation was conducted using a 2D/3D soil-water coupled finite element method program named as DBLEAVES [4]. The applicability and the accuracy of the program have been firmly verified by shaking table tests and other various liquefaction phenomena [5]-[8].

CM model is adopted to simulate the static/dynamic behavior of the non-cohesive soils in the current study. CM model can consider the effect of the stress-induced anisotropy, the density and the structure of soils in a unified way. It can properly describe the mechanical behaviors of non-cohesive soils subjected to monotonic/cyclic loading under drained/undrained conditions. Based on the concepts of subloading [9] and superloading [10], the subloading, normal and superloading yield surfaces in *p*-*q* (mean principal stress - deviatoric stress) plane are adopted in the model to take into consideration the influence of density and the structure of soil, as shown in Figure 1.

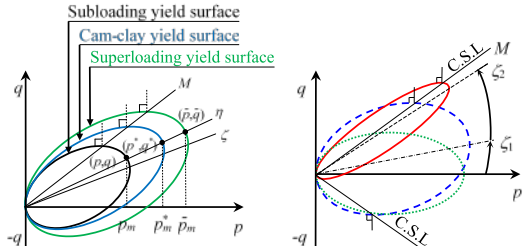

Fig.1 Yield surfaces and its change with the development of anisotropy

2.1 The Second Level Headings

Besides, the elliptical yield surfaces may change with the development of the stress-induced anisotropy. These characteristics enable the model to describe the cyclic mobility of non-cohesive soils. Eight parameters are employed, among which five parameters are the same as those in the Cam-clay model [11]. The others are a parameter for controlling the collapse rate of the structure, losing rate of the overconsolidation ratio and the developing rate of the stress-induced anisotropy. All parameters have clear physical meanings and can be easily determined by undrained triaxial cyclic loading tests and drained triaxial compression tests. A detailed description and applicability of CM model can be found in the reference [3]-[8].

In the analysis with DBLEVES, the dynamic /static analyses are conducted using the same program, the same parameters throughout the whole calculating process. Newmark-β method is used and the integration time interval is 0.005 sec. Integration time interval is decided from interval time of observed earthquake motion and previous studies. Since it is expected that strong nonlinearity of the soil would occur, Rayleigh type of initial-rigidity-proportional attenuation is adopted and the damping values of the soils, the structure, and the piles are assumed to be 2% and 10% for the first and second modes respectively. Before dynamic analyses of earthquake motions, a gravitational stress field analysis is carried out to obtain the initial effective stress on the ground.

3. NUMERICAL SIMULATION DURING AND AFTER EARTHQUAKE

3.1 Earthquake waves

A typical two directions earthquake motion at Simousa 2300m below the ground surface at Chiba Prefecture was recorded and it is selected to be the input earthquake motion in present analyses as shown in Figure 2.

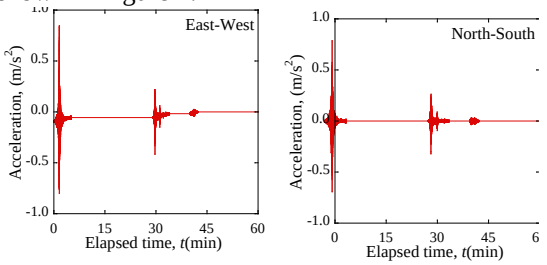

Fig.2 Recorded seismic motions at Shimous (K-Net, http://www.k-net.bosai.go.jp)

It is noted that the earthquake with the main shock followed by two aftershocks shakes in E-W and N-S directions at the same time. The main shock lasted for 300 seconds with a maximum acceleration of 0.85 m/s^2 and the first aftershock also lasted for 300 seconds with a maximum acceleration of 0.25 m/s^2 while the second aftershock lasted for 135 seconds with a maximum acceleration of 0.04 m/s^2.

The interval between the main shock and the first aftershock was approximate 24 minutes and the interval between the two aftershocks was approximate 6 minutes. It should be mentioned herein that such a long duration of motions has been expected to be the major cause of the severe liquefaction and ground deformation.

3.2 Simulation for one column ground

3.2.1 Simulation scenario

The following 3 cases are considered to evaluate the influence of the main shock on its aftershocks and visa verse:

Case 1: Calculation is conducted in the same way just as the scenario happened in the Great East Japan Earthquake: (1) main shock, (2) 1440 seconds consolidation, (3) first aftershock, (4) 360 seconds consolidation, (5) second aftershock, (6) consolidation until the settlement of the ground ceased completely (50 years).

Case 2: Calculation is conducted only considering the main shock and consolidation after the main shock for a comparison with Case 1: (1) main shock, (2) consolidation until the settlement of the ground ceased completely.

Case 3: Calculation is conducted only considering the aftershock-1.

3.2.2 Investigated site and analyses mesh for FEM

The investigated site was reclaimed by dredged soils that consist predominantly of sand or silt from the seabed of Tokyo Bay. Figure 3 shows the result of a boring survey in the investigated site and the corresponding FEM mesh used in the calculation.

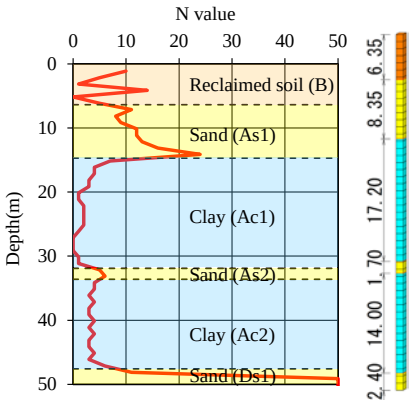

Fig.3 Geological profile and FEM mesh

The mesh is coincident with the boring data. It is one column ground with a 1.0m x1.0m horizontal square area. Each mesh has the depth of 1m. In the case of dynamic analyses, an equal-displacement boundary, or called as periodic boundary, is applied to two side boundaries in *x*- and *y*-directions respectively to deal with the artificially introduced boundaries that do not exist in reality so that the incident waves are always allowed to transmit freely from the artificial boundaries introduced in FEM analysis in finite domain. The bottom is assumed to be fixed in horizontal and vertical directions. The drained boundary (groundwater level) is set at the ground surface.

3.2.3 Material parameters

The material parameters used in the calculation are shown in Table 1, and Figure 4 shows the theoretical estimation of the element behavior in undrained cyclic loading test. Since no cyclic testing data of soils are available, some of these parameters were determined with reference to the standard penetration tests, and others were estimated with reference to those of *Toyoura* sand. From the results, it is known that the strain accumulates as the number of cyclic loading increases, and liquefaction accompanied by cyclic mobility may occur in the reclaimed layer (B) and loose sand layer (As) at the investigated site. However, liquefaction will not occur easily in the loose silt layer (Ac).

Table 1 Material parameters

	B	As1, 2	Ac1, 2
Compression index λ	0.050	0.030	0.043
Swelling index κ	0.0064	0.0060	0.0090
Passion's ratio ν	0.300	0.300	0.300
Stress ratio at critical state R_f	3.650	3.650	3.000
Void ratio e_0 (p'=98kPa on N.C.L)	0.870	0.870	0.920
Degradation parameter of structure a	2.200	2.200	0.100
Evolution parameter of anisotropy b_r	1.500	1.500	0.100
Degradation parameter of over-consolidation m	0.100	0.100	2.200
Unit weight γ (kN/m^3)	17.64	17.64	16.66
Permeability k (m/s)	1.0E-4	1.0E-4	1.0E-9
Initial structure R^*_0	0.800	0.800	0.600
Initial degree of over-consolidation $1/R_0$	4.000	2.500	1.500
Initial anisotropy ζ	0.000	0.000	0.000

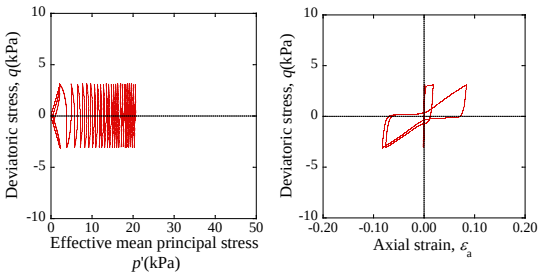

(a) Reclaimed layer (B layer, GL-3.50m)

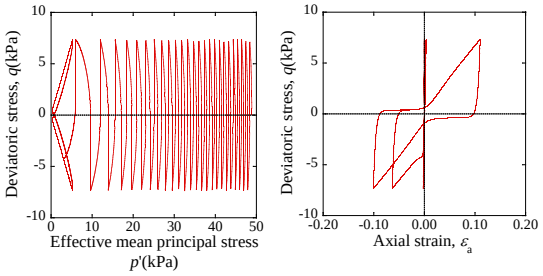

(b) Loose sand (As layer, GL-10.50m)

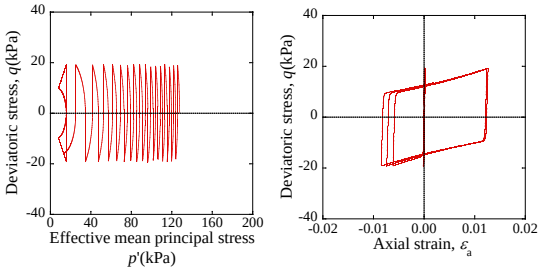

(c) Loose silt (Ac layer, GL-22.50m)

Fig.4 Effective stress paths and stress-strain relations

3.2.4 Results and discussions

Figure 5 shows analysis results of the excess pore water pressure ratio (EPWPR) in the Case 1 and 3. Case 1 has a history of the main shock before the aftershock-1 while Case 3 did not have a history of the main shock. Here, EPWPR is defined as the ratio of excess pore water pressure to the initial vertical effective stress. Therefore, EPWPR equaling to 1 means liquefaction.

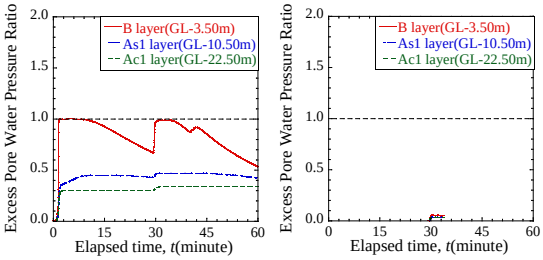

(a) Case 1 (b) Case 3

Fig.5 Results of the excess pore water pressure ratio

From the result, in the Case 1, for the sand (As1) and the clay (Ac1), liquefaction did not occur in the main shock but excess pore water pressure (EPWP) kept increasing after the aftershocks because of the constant water supply from the lower layers. For the reclaimed layer (B), EPWPR increased up almost to 1 both in the main shock. And after the main shock, EPWPR of the reclaimed layer (B) decreased to about 0.70, but liquefaction occurred again in the aftershock-1 even though the maximum acceleration of the aftershock-1 is less than 25 gal. On the other hand, an increasing of EPWPR of Case 3 is much smaller than that of Case 1. Therefore, when a ground has not recovered from damage by the main shock, a liquefaction easily occur by a small aftershock. From the above results, it is known that the accumulation of EPWP and development of stress-induced anisotropy induce ground liquefaction.

Figure 6 shows a comparison of ground surface settlements after earthquake between the Case 1 and 2. In order to investigate the influence of aftershocks on the long-term settlement due to the consolidation of ground, the simulation was conducted. The Case 1 has a history of the aftershocks but Case 2 did not have that. From the results, ground surface settlement of Case 1 with aftershocks than Case 2 without that. It can be concluded that both the liquefaction and the settlement are significantly affected by the aftershocks.

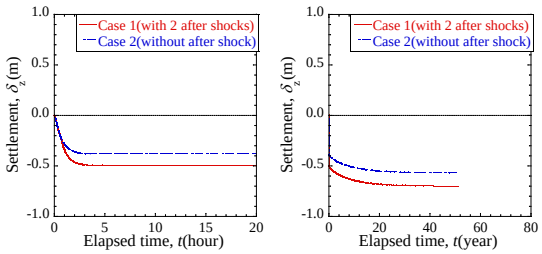

(a) 0 to 20 hours (b) 0 to 50 years

Fig.6 Ground surface settlements in Case 1 and 2

3.3 Simulation for three-dimensional ground

3.3.1 Simulation scenario

In above simulation (Case 1) for one column ground, the calculation is conducted in the same way just as the scenario happened in the Great East Japan Earthquake: (1) main shock, (2) 1440 seconds consolidation, (3) first aftershock, (4) 360 seconds consolidation, (5) second aftershock, (6) consolidation until the settlement of the ground ceased completely (50 years).

3.3.2 Investigated site and analyses mesh for FEM

Figure 7 shows the plan view of the soil distribution based on the results of Swedish weight sounding test.by the inhabitants during six months after the earthquake. Soil conditions in this area were also investigated by in-situ boring combined with the Standard Penetration Test (SPT), prior to and after the earthquake. According to the results of SPT and the Swedish weight sounding test, the whole area can be divided into three types of soil, that is, type A, type B and type C. Based on the results shown in Figure 7, the investigated site in the analysis can be divided into four areas.

The dimension of the calculated area in FEM is 400m in length, 300m in width and 50m in depth, as shown in Figure 8. As to boundaries between different types of soil, transition zones were set to link the different types of soil as indicated in soil type AC, type AB, type BC, type ABAC, type BCBA and type CACB.

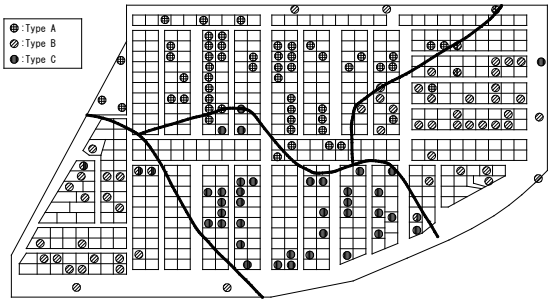

Fig.7 Plan view of the soil distribution based on the results of Swedish weight sounding test

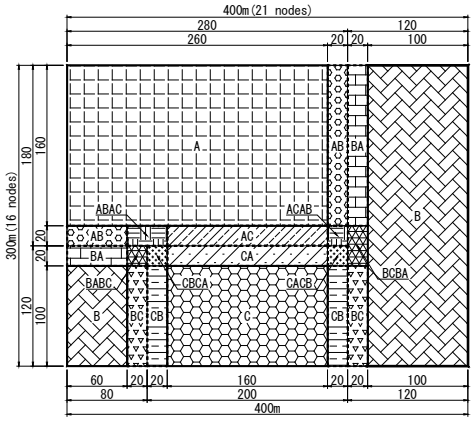

Fig.8 Plan view of the calculated area in FEM

Figure 9 shows the geologic profiles of the calculated area. All geologic profiles consist of loose sand and loose silt above G.L. -15m. The loose sand layer near the surface has an SPT N-value of 5~15 and it easily causing liquefaction.

Figure 10 shows the finite element mesh. As for the mesh size, the whole depth of calculation area is 50 m, the top 16 m is divided into 16 layers with each layer of 1m thickness and the below 34 m is divided into 17 layers with each layer of 2 m thickness. In the analyses, the elements in each soil layer at the center of type A, type B (the larger part) and type C area are selected. In the case of dynamic analyses, an equal displacement boundary condition is applied for two side boundaries in *x*- and *y*-directions respectively to deal with the energy dissipation problem. The bottom is assumed to be fixed in all directions. The drained boundary is set at the ground level of -1 m.

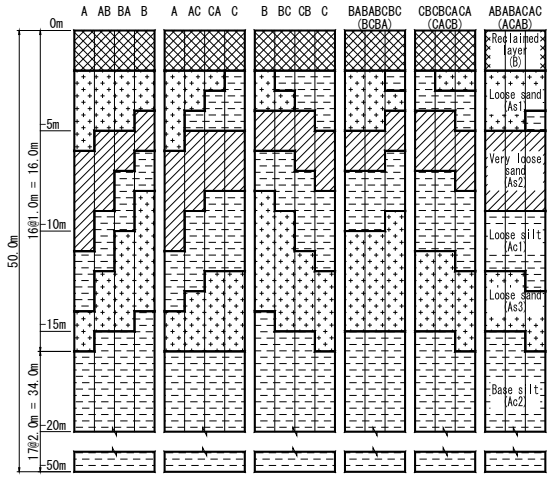

Fig.9 Geologic profiles of the calculated area

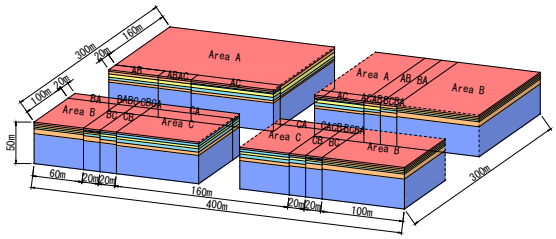

Fig.10 Finite element mesh

3.3.3 Material parameters

The material parameters used in the calculation are shown in Table 2, and Figure 11 shows the theoretical estimation of the element behavior in undrained cyclic loading test. Even in this calculation, since no cyclic testing data of soils are available, some of these parameters were determined with reference to the results of SPT, and others were estimated with reference to *Toyoura* sand. From the analyses results, it is known that the strain accumulates as the number of cyclic loading increases, and liquefaction accompanied by cyclic mobility may occur in the reclaimed layer, loose sand and very-loose sand except for loose silt land the base silt.

Table 2 Material parameters

	B	As1	As2	Ac1	Ac2
λ	0.030	0.030	0.043	0.207	0.207
κ	0.006	0.006	0.009	0.041	0.041
ν	0.300	0.300	0.300	0.350	0.350
R_f	4.600	4.600	4.600	3.500	3.500
e_0	0.720	0.720	0.880	1.100	1.100
a	2.200	2.200	0.100	0.100	0.100
b_r	1.500	1.500	0.100	0.100	0.100
m	0.100	0.100	0.100	3.800	3.800
γ (kN/m^3)	17.60	18.00	17.00	15.40	17.70
k (m/s)	1.0E-5	1.0E-5	1.0E-6	1.0E-7	1.0E-7
R^*_0	0.800	0.800	0.600	0.600	0.600
$1/R_0$	5.000	5.000	3.000	2.500	2.500
ζ	0.000	0.000	0.000	0.000	0.000

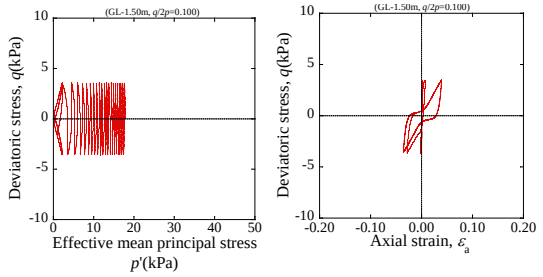

(a) Filled soil in reclaimed layer (GL-1.50m)

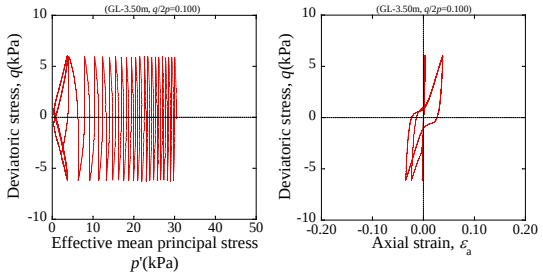

(b) Loose sand (GL-3.50m)

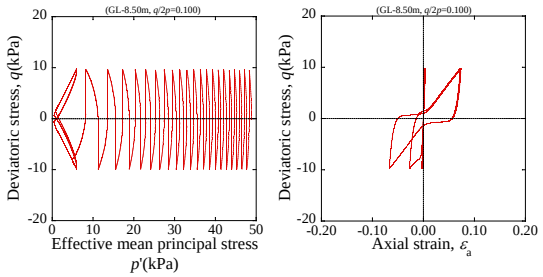

(c) Very loose sand (GL-8.50m)

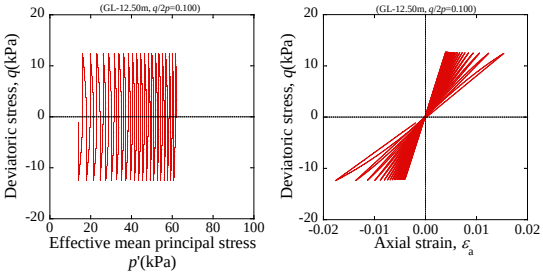

(d) Loose silt (GL-12.50m)

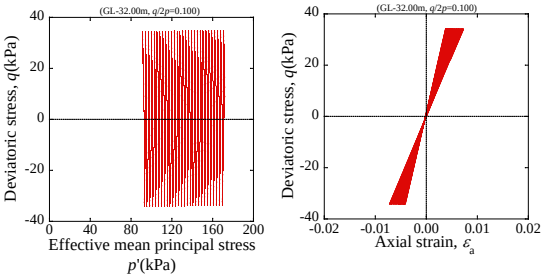

(e) Base silt (GL-32.00m)

Fig.11 Effective stress paths and stress-strain relations

3.3.4 Results and discussions

Figure 12 shows the EPWPR with time in different soil layers at the center of type A, type B, and type C respectively. For the upper loose sand (As1) in the area of type A, liquefaction did not occur in the main shock, but that occurred in after shock. In the area of type B, however, EPWPR in aftershock is smaller than that of the main shock. For the very loose sand (As2) in the areas of type A and B, EPWPR raised up almost to 1 in the aftershocks although they were much smaller than the main shock. In the area of type C, however, liquefaction occurred seriously in both the main shock and aftershocks. For the loose silt (Ac1), it did not liquefy anyhow but EPWP kept increasing after the aftershocks because of the constant water supply from the lower layer of whole ground. For the lower loose sand (As3) in the area of type B, liquefaction occurred in the main shock and although EPWP decreased somehow after the main shock the ground liquefied again in the aftershocks. In the areas of type A and C, however, EPWPR was smaller than that of type B.

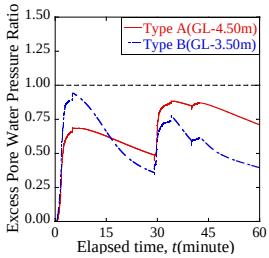

(a) Loose sand (As1)

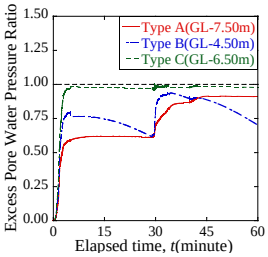

(b) Very loose sand (As2)

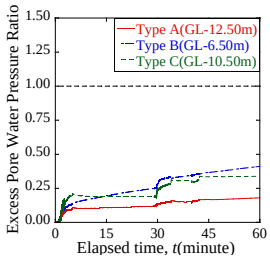

(c) Loose silt (Ac1)

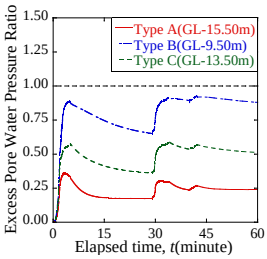

(d) Loose sand (As3)

Fig.12 Excess pore water pressure ratios

Figure 13 shows the distribution of EPWPR at different depths. The left side of the figure is the EPWPR immediately after the main shock and the right of the figure is the EPWPR immediately after the aftershock-1. At the depth of 6m below the ground surface, liquefaction area due to the main shock was clearly smaller than that of the aftershock. In other words, liquefaction occurred in the aftershock was more serious than that of the main shock in the area of type A and type C. At the depth of 8m below the ground, liquefaction only occurred in the area of type A after the aftershock.

In general, the EPWPR in all areas and soil types may increase again in the aftershock.

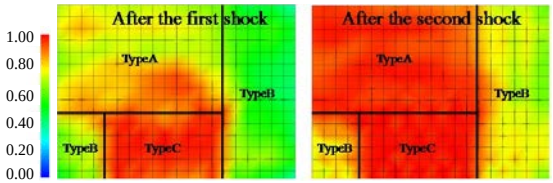

(a) GL-6.00m

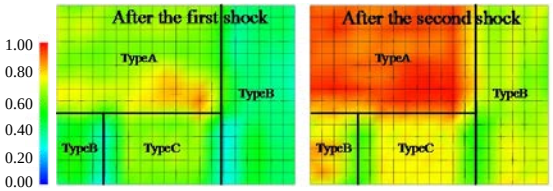

(b) GL-8.00m

Fig.13 Distribution of EPWPR at different ground levels (Left: main shock, Right: aftershock-1)

Figure 14 shows the calculated distribution of settlement of ground surface. Six hours after the earthquake, an uneven deformation appeared in the area of type C. In this area, the maximum amount of upheaval of the ground reach about 0.5m while the ground in types A and B settled about 0.5m. This uneven ground settlement was observed extensively in the field survey. Photo 1 shows the uneven settlement in roadways near the observed site. However, according to the analyses, the ground of all areas will turn out to be settled down 0.25m to 0.90m in 50 years after the earthquake, as shown in Figure 14 (b).

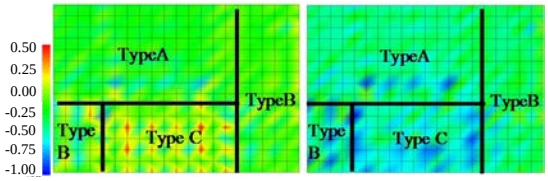

(a) 6hours (b) 50 years

Fig.14 Distribution of settlement of ground surface

(a) Surface of sidewalk (b) Heaved sidewalk

Photo 1 Uneven settlement near the observed sites

3.3.5 X-ray CT image of geological features

Figure 16 shows the photograph and X-ray CT images of core sections drilled immediately after the liquefaction at calculated area [12]. A very important result we have got in this research is that the liquefied soil strata were perfectly identified with X-ray CT images. The pink line next to the CT image indicates the liquefied soil layers that distributed at the depth of 6.2m to 8.6m, where the thin strata of reclaimed ground that was observed clearly at the up strata from 2.0m to 6.2 m, suddenly disappeared due to the liquefaction. This observed phenomenon was remarkably similar to the calculated results showed in Figures 13, 14. It is therefore reasonable to say that the analysis method based on CM model, used in this sturdy, can well describe the actual situation of the liquefaction in the main shock, the re-liquefaction in the aftershock, and the consolidation settlement of ground after multiple earthquakes.

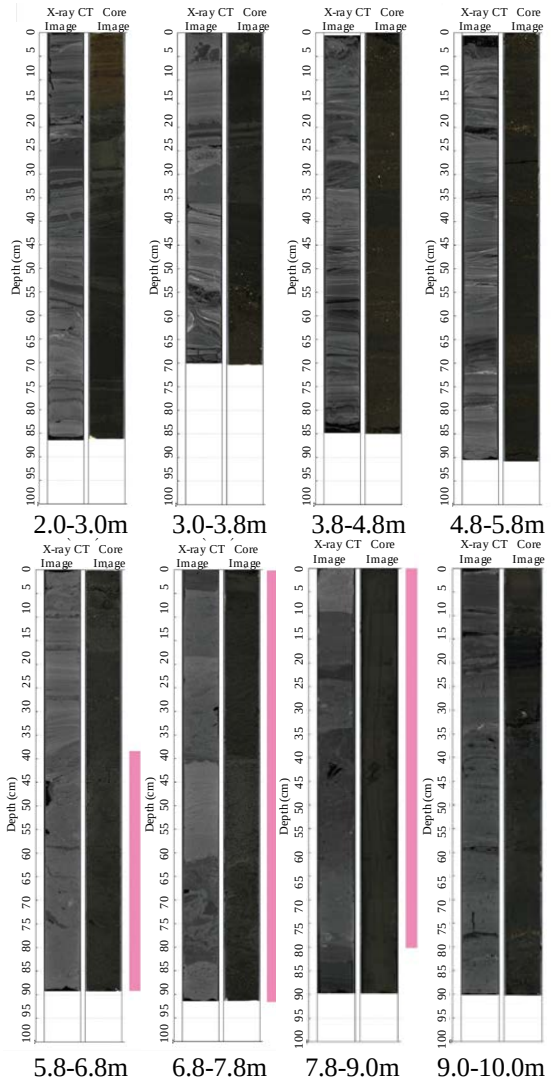

Fig.16 Photograph and X-ray CT images of core sections drilled in calculated area after liquefaction

4. CONCLUSION

In this study, 3D soil-water coupled finite element-finite difference analyses based on CM model were conducted to investigate the mechanism of liquefaction and consolidation settlement of ground in multiple earthquakes. The following conclusions can be obtained:

1. According to the calculated results of the liquefaction and the settlement in simulation for one column ground and three-dimensional ground, residual excess pore water pressure and stress-induced anisotropy have a big influence on the subsequent ground behavior.

2. When a ground receives the damage from the main shock and could not recover promptly, excess pore water pressure in low permeability soil remains high and the stress-induced anisotropy develops to a large level. As a result, liquefaction may be caused again even by a small aftershock.

3. When an earthquake occurs at ground having low permeability soil, excess pore water pressure may cause not only immediate settlement but also long-term settlement due to consolidation.

4. By the comparison between the calculated results and the field observation, it is known that the calculations are consistent well with the real liquefaction and settlement behavior.

5. REFERENCES

[1] Kazama M., Overview of the damages of The 2011 Off the Pacific Coast of Tohoku Earthquake and its geotechnical problems, Japanese Geotechnical Journal, Vol. 7, No. 1, 2012, pp. 1-11.

[2] Oka F., Yoshida N., Kai S., Tobita T., Higo Y., Torii N., Kagamihara S., Nakanishi N., Kimoto S., Yamakawa Y., Touse Y., Uzuoka R. and Kyoya T., Reconnaissance Report of Geotechnical Damage due to the 2011 off the Pacific coast of Tohoku Earthquake - Northern Area of Miyagi Prefecture -, Japanese Geotechnical Journal, Vol. 7, No. 1, 2012, pp. 37-55.

[3] Zhang F., Ye B., Noda T., Nakano M. and Nakai K., Explanation of Cyclic Mobility of Soils: Approach by Stress-Induced Anisotropy, Soils and Foundations, Vol.47, No. 4, 2007, pp. 635-648.

[4] Ye B., Experiment and Numerical Simulation of Repeated Liquefaction -Consolidation of Sand, Doctoral Dissertation, Gifu University, 2007.

[5] Morikawa Y., Bao X., Maeda K., Imase T. and Zhang F., Importance of liquefaction analysis considering re-liquefaction due to aftershock of earthquake, Japanese Geotechnical Journal, Vol. 7, No. 2, 2012, pp. 389-397.

[6] Zhang F., Oka R., Morikawa Y., Mitsui Y., Osada T., Kato M. and Wabiko Y., Shaking Table Test on Superstructure-foundation-Ground System in Liquefiable Soil and Its Numerical Verification, Geotechnical Engineering Journal of the SEAGS & AGSSEA, Vol. 45, No. 2, 2014, pp. 1-6.

[7] Morikawa Y., Tanaka Y., Maeda K. and Cho H., Countermeasure against liquefaction using drainage diaphragm wall focused on the effect of dissipation of water pressure, Journal of JSCE, Ser. A2, Vol. 71, No. 2, 2015, pp. I_437-I_448.

[8] Hamayoon K., Morikawa Y., Oka R., Zhang F., 3D dynamic finite element analyses and 1 g shaking table tests on seismic performance of existing group-pile foundation in partially improved grounds under dry condition, Soil Dynamics and Earthquake Engineering, Vol. 90, 2016, pp. 196-210.

[9] Hashiguchi K. and Ueno M., Elastoplastic constitutive laws of granular material, Constitutive Equations of Soils, Pro. 9th Int. Conf. Soil Mech. Found. Engrg., Spec. Ses. 9, Murayama, S. and Schofield, A. N. (eds.), Tokyo, JSSMFE, 1977, pp. 73-82.

[10] Asaoka A., Nakano M., Noda T., Superloading yield surface concept for the saturated structured soils, Proc. of the Fourth European Conference on Numerical Methods in Geotechnical Engineering-NUMGE98, 1998, pp. 232-242.

[11] Roscoe K. H., Schofield A. N. and Thurairajah A.: Yielding of clays in states wetter than critical, Geotechnique 13 (3), 1963, pp. 211-240.

[12] Taira A., Iijima K., Igarashi C., Sasaki S., Sakaguchi H., Sakaguchi A., Kikawa E., Kanamatsu T., Yamamoto Y., Azuma W., Tanaka T., Nishimura M., Suzuki T., Kido Y., Watanabe N., Okuno M., Inoue T., Mayuzumi H., Oda T., Hamada T., Muroyama T., Takeo I., Takashina J., Katsumata H., Harada N., Nishida F., Minamikawa H. and Kanetaka Y., Identification of a Soil Liquefied Layer due to the 2011 off the Pacific Coast of Tohoku Earthquake Using X-ray CT Scan Imaging: An Example from Core Samples from Maihama 3-chome, Urayasu City, The Journal of the Geological Society of Japan, Vol. 118, No. 7, 2012, pp. 410-418.